Hindawi
International Journal of Geophysics
Volume 2023, Article ID 6633599, 11 pages
https://doi.org/10.1155/2023/6633599

Research Article

GPR and Magnetic Techniques to Locate Ancient Mining Galleries (Linares, Southeast Spain)

Rosendo Mendoza,[1] **Bruna Marinho**,[2] **and Javier Rey**[2]

[1]*Dpto. de Ingeniería Mecánica y Minera y CEACTEMA, EPS de Linares, Universidad de Jaén, Campus Científico Tecnológico, 23700 Linares, Jaén, Spain*
[2]*Dpto. de Geología y CEACTEMA, EPS de Linares, Universidad de Jaén, Campus Científico Tecnológico, 23700 Linares, Jaén, Spain*

Correspondence should be addressed to Javier Rey; jrey@ujaen.es

Received 18 April 2023; Revised 18 June 2023; Accepted 13 August 2023; Published 30 August 2023

Academic Editor: Angelo De Santis

Old mining districts have created numerous subsurface cavities, often at shallow depths. The resulting subsidence risk is a major territorial planning problem, especially when these holes are in urban expansion areas. Ground-penetrating radar (GPR) and magnetic techniques can help to detect and to characterise these shallow mining structures based on the strong contrast of electromagnetic and magnetic properties (dielectric constant and magnetic susceptibility) between the rock and the backfill of cavities. In the present study, these techniques were used to locate old mining cavities near the city of Linares, located south of Spain and connected to the area's old mining district. GPR and magnetometry (total magnetic field and vertical magnetic gradient) were performed on a grid in one of the most important veins in the sector. By comparing both working methods, the vein structure within the granite can be detected. On the one hand, the magnetic prospecting technique (magnetic anomalies) has allowed us to detect when the vein is covered by metallic elements of natural or anthropogenic origin. On the other hand, strong reflections and hyperbolic events associated in GPR profiles confirm the presence of cavities related to old mining operations. Shallow magnetic anomalies not associated to GPR variations are related to the slag present in the study area (detected in the outcrop) or to unexploited vein mineralizations.

1. Introduction

The Linares metallogenic district (Southeast Spain, Figure 1) is characterised by its vein-type deposits, primarily composed of galena (PbS) and hosted within a Palaeozoic basement. This Palaeozoic basement comprises a granitic batholith intruded into pelitic facies [1, 2]. The basement and the vein-type deposits are covered by Triassic sandstones and red lutites (New Red Sandstones) and by Quaternary alluvial facies.

The district was subjected to intensive mining from Roman times until the late 1970s when the mines were closed and abandoned. Currently, this district has two notable features, namely, subsurface cavities derived from mining and relatively vast swathes of ruins of abandoned mining buildings and mineralogic and metallurgic waste heaps.

The subsurface cavities reach depths of 600 m, storing groundwater within an impermeable set [3]. Currently, most of this volume is flooded. For this reason, the batholith is hydrogeologically important because its exploitation enables groundwater extraction at pumping flows ranging from 30 to 50 L/s [4].

The rational exploitation of this resource is crucial for the agricultural development of the county. Developing a hydrodynamic model for this batholith requires knowing the spatial structure of these underground workings. For this purpose, these mining cavities have been reconstructed by applying image analysis techniques to mine workings [5], thereby estimating a volume of 13 Hm^3 of cavities [6].

However, these cavities, especially the shallowest cavities, may cause surface subsidence and surface deformations. In

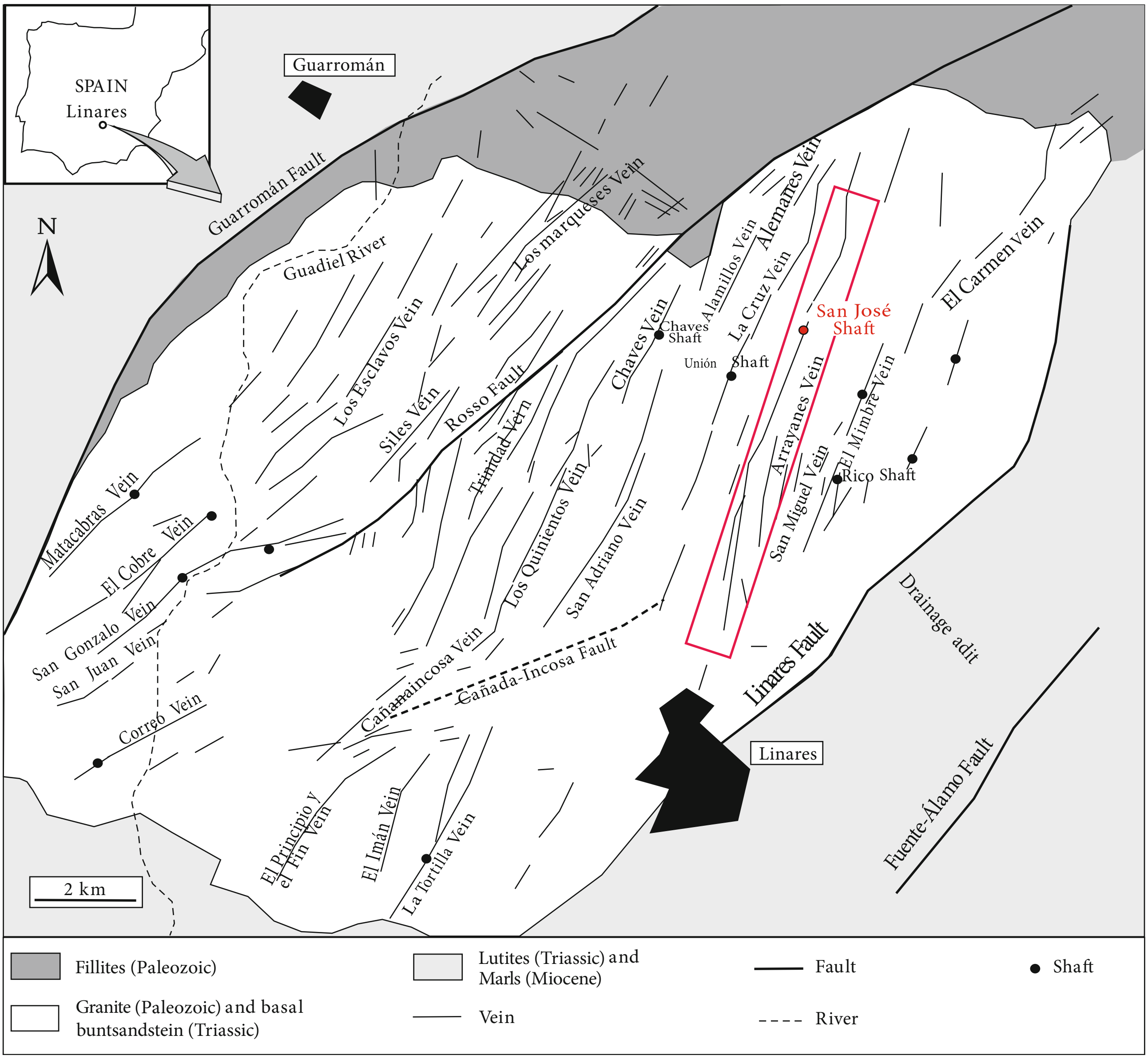

Figure 1: Geographical and geological location of the studied region. The box highlights the position of the Arrayanes mining concession. The San José well also stands out.

this sense, important subsidence and collapse phenomena have recently occurred in the vicinity of the city. Sinkholes, with sizes that sometimes exceed tens of meters in diameter and depth, have been generated in relation with the old mining operations. This has aroused a great social alarm.

Given the risk of subsidence associated with old mines, these mine workings must be carefully considered in the territorial planning of the county, particularly when deciding the location of buildings requiring minimum guarantees of stability. As a case in point, the oldest mines are located within 10 m of the surface, and their age remains unknown. Broadly, they are cavities partly filled with gangue (loose granite stones) and Triassic clays dragged by water from the surface. They may also contain unexploited mineralization or abandoned elements used for mineral extraction. In this sense, large subsidences have recently occurred in the sector associated with the traces of seams.

The present study is aimed at locating these old shallow mine workings using geophysical techniques. Contrasts in the physical properties can be used to identify the feature geometries. These properties, such as magnetic susceptibility density, electrical resistivity, and conductivity, vary between the media involved.

In this paper, two geophysical (GPR and magnetic) techniques have been used. The goal of this study was to compare the different results to determine the usefulness of these indirect techniques for locating the trace of shallow mining cavities embedded in the granite and to determine whether they are filled with air or other elements. This study was conducted in the former Arrayanes mining concession, associated with the San José vein (Figure 1), one of the most important of the district, showing surface subsidence. The use of these tools may be extrapolated to the detection of other cavities, such as mine galleries or karstic cavities [7, 8], which could be highly useful when designing buildings.

2. Regional Setting

The Linares mining district encompassed an impressive network of concessions (totalling 1,011 in 1890), whose borders and names have varied over the years [9]. Among these concessions, the "Arrayanes concession" stood out for its richness in minerals and its long history as the most emblematic in the sector. This rectangular concession is located a few kilometers northeast of the city of Linares (Figure 1), in the north-23°-east direction, running parallel to the veins. Within the vein unit, the mineralizations were concentrated in enriched areas into lenticular deposits. Although mainly galena (PbS) was exploited, paragenesis also showed other minerals such as sphalerite (ZnS), pyrite (FeS_2), chalcopyrite ($CuFeS_2$), argentite (Ag_2S), ankerite ($Ca[Mg,Fe][CO_3]_2$), quartz (SiO_2), and barite ($BaSO_4$) [1, 10, 11]. The concentration of these minerals was very variable in the trace of the vein, which conditioned the economic interest and, therefore, its exploitation. The mine workings were concentrated in four subvertical granite-hosted veins: the main vein, also known as the San José vein, San Ignacio, Zulueta, and, finally, Ocharán, which was also known as Endrina.

The study was conducted in the San José vein near the San José shaft (Figure 2). This vein was intensely exploited in the second half of the 19th century in area and depth. Thus, the San José shaft was only 102 m deep in 1876 but reached 617 m by 1931. According to available information on the work plans, the levels were approximately 25 m apart. The first level was around 20 m deep, and the 20th level was approximately 500 m deep [9]. However, much older mine workings, some of which date back to Roman times, with very primitive methods, were usually very shallow (less than 10 m deep) and were discontinued, exclusively limited to the most galena-enriched sectors of the vein. These mine workings were the focus of our study because they are superficial, posing a higher risk of subsidence. The results highlighted these processes in outcrops near this shaft, along the vein (Figure 3(a)).

3. Material and Methods

3.1. Ground-Penetrating Radar (GPR). The GPR technique is based on the propagation and reflection of high-frequency (10 MHz-2.5 GHz) electromagnetic waves in the subsurface. GPR devices have a transmitter antenna, which is moved over the ground surface, emitting very short pulses. When these waves encounter a dielectric contrast in the subsurface, they are reflected towards the surface, where their characteristics are measured by a receiving antenna [12]. The penetration depth and resolution depend on the electromagnetic properties of the materials and the antenna. Thus, wave propagation in the subsurface decreases with increasing ground conductivity or signal frequency. In the same profile, high-frequency antennas provide high resolution and shallow penetration depth and vice versa when using low-frequency antennas [13]. Electric and magnetic fields propagate through a conductor (in this instance, the ground) at varying depths, with the electric field experiencing quicker decay than the magnetic field. The skin depth is the measure of distance at which the electric field has reduced to roughly $1/e$ (about 37%) of its surface value [14]. Knowledge of the skin depth can assist in identifying the suitable frequency range for a given survey in detecting features at the desired depth. Additionally, this information aids in optimizing antenna design and signal processing parameters [14, 15]. This method has been described in detail in several previous studies [13, 14, 16, 17].

GPR prospecting method has been widely used in geoscience studies, including studies focused on surface geology, hydrology, mining, environment, forensics, and archaeological or heritage studies [7, 15, 17, 18]. In this sense, Cardarelli et al. [19] applied this technique successfully in civil engineering to evaluate the rock fracturing and obsolescence of the concrete lining in a tunnel. In archaeology, there are numerous examples in which the use of GPR has allowed the location of buried cavities [20]. On the other hand, an important GPR application is the localization of karstic morphologies as cavities and buried sinkholes [8, 21–23]. The device used in this study (Figure 3(b)) was the RAMAC/GPR system, Pro-Ex model, manufactured by MALA GEOSCIENCE (http://www.malags.com/home). GPR profiles were acquired with a 250 MHz shielded antenna (Figure 3(b)) and processed in data acquisition software, Ground Vision (https://wwwguidelinegeoc.cdn.triggerfish.cloud/uploads/2016/07/MALA-Ground-Vision-v.2.1.pdf). This software enables us to set, for each record, the measurement parameters and thus the sampling frequency of the antenna, the time window, and the number of samples per trace or zero time.

3.2. Magnetic Prospecting. Magnetic prospecting is a passive geophysical technique based on the detection of local variations (anomalies) in the Earth's magnetic field, usually expressed in nT. These anomalies are caused by materials with high magnetic susceptibility; that is, they can become magnetised by the Earth's magnetic field. Before their interpretation, these measurements must be corrected for diurnal variations in the magnetic field using an auxiliary station. This auxiliary station is used to periodically compare the measurements or as a reference based on its variations. This method has been extensively described in literature [14, 15, 24].

Widely used in various fields of Earth sciences, magnetic prospecting is a classical tool, useful in the geological mapping of large, covered or inaccessible areas, in hydrocarbon exploitation [25], or in prospecting metallic ore mineralization [26–28]. This line highlights the work of Gobashy et al. [29] and Eldougdoug et al. [30] that used geophysical aeromagnetic and geological studies to explore gold mineralization in altered ultramafic rocks in Egypt. They detected the mineralizations linked to faults with a low magnetic susceptibility response. Recently, gradiometry has also been used. This technique comprises simultaneously using two magnetic sensors placed at different heights (normally separated by approximately 0.5 to 1 m) to measure the difference in the total magnetic field between the two sensors [15]. The vertical magnetic field gradient is expressed in nT/m. This technique does not require diurnal corrections because the

FIGURE 2: Aerial photograph showing the position of the studied grid next to the San José mine, in the Arrayanes mining concession. The supposed position of the vein trace is also marked.

two sensors are equally affected by the external magnetic field, which is one of the main advantages of this technique. Gradiometer measurements highlight shallow anomalies; that is, they are less sensitive to deep anomalies, thus opening new applications such as doline or karstic cavity detection [7, 22], archaeological prospection [18, 31], environmental studies [32], and detection of unexploded ordnance in military zones [33].

In this study, fieldwork was performed using a portable GSMP-35G Potassium Magnetometer/Gradiometer, v8.0, GEM System (Figure 3(c)). This potassium magnetometer/gradiometer offers high-quality data because of its high sensitivity (0.0003 nT), minimal reading error, resolution (0.0001 nT), and high precision (±0.05 nT). It can take up to 20 readings per second, which gives a remarkable sampling density while walking. A calculation of total magnetic field anomalies was performed using a standard procedure, including reduction to the IGRF 13 (https://geomag.bgs.ac.uk/data_service/models_compass/igrf_calc.html). In the magnetometry study, the reference used to correct the diurnal variation was the permanent magnetic station located in San Pablo (Toledo, Spain; https://www.ign.es/web/gmt-magneto-san-pablo).

4. Geophysical Data Acquisition

4.1. GPR Data Acquisition. A grid was designed, measuring 29 (X-direction) by 47 (Y-direction) m, with a 1 m interval between GPR profiles. In total, 30 profiles were acquired in the Y-direction. The position of the grid near the San José mine is indicated in Figure 2, showing the possible location of the old vein, which can be traced in aerial photographs by aligning mining remnants in the area and sometimes overlaps with sinkholes.

In this survey, all profiles were acquired with a 250 MHz shielded antenna, with 0.018 m trace spacing and a 70 ns time window (512 samples per trace). The signal recorded in the field was processed using Reflexw software [34]. First, a start timing static correction filter was used to adjust the delay time of the first wave arrival. Electromagnetic wave velocity in these materials was calculated by adjusting diffraction hyperbolas (option velocity adaptation). A subtract DC shift filter was used to remove residual voltage, and background removal and subtract mean (dewow) filters were used to remove the direct wave. Main gain adjustments were made in the Y-axis to amplify the signal. Finally, a bandpass frequency filter was used to remove high and low frequencies.

4.2. Magnetic Data Acquisition. The magnetic survey was performed in the 29×47 m grid described in the previous section (Figure 2). A continuous profile was acquired (the walking mode of the device) in a Cartesian coordinate system, with parallel lines in the Y-direction, in 1 m increments and reference stations every meter along the profile. Given the stability of the equipment used, measurements were taken every 50 ms. The vertical pseudogradient magnetic

(a) (b) (c) (d)

Figure 3: Recent sinkholes in the Linares mining district, close to the urban area. In the photograph, an inverted cone morphology of more than 15 m in diameter and about 30 m deep (a); GPR study in sector (b); magnetic study in sector (c); remains of foundry slag observed in the grid studied (d).

method was used for the data acquisition, with two separate sensors 0.5 m apart and the lowest being 0.2 m above ground level.

To avoid distortions in the measurements, the ground surface was cleaned in advance to remove anthropic elements. However, it was impossible to remove all scattered remains of smelting slag, which are particularly abundant on the southwest margin of the grid (Figure 2). Some of these remains are shown in the photograph in Figure 3(d).

5. Results and Discussion

5.1. GPR Data. Figure 4 shows five of the 30 profiles that were acquired in this study. Using Reflexw software, reflection hyperbolas were analyzed, thereby estimating a wave velocity of 0.952 m/ns in these lithologies. In all profiles, the contact between the top of the granitic batholith (in which the veins are hosted) and the Triassic base comprising sandstones and clays hosting mineralizations is indicated with a red-dashed line. Although the contact surface is irregular, it is usually approximately 1 m deep in this area. This information is confirmed by direct observations in the field.

In profile 1, at approximately 6-8 m from the origin, the radargram displays hyperbolic events associated with the presence of a cavity at a depth of approximately 1.5-2.0 m, near the contact between the granite and Triassic sandstones. The strong dielectric contrast between the granite and the cavity fill (air or soil material) may explain this response. Between 22 and 26 m from the origin and at equivalent depths, strong reflections and hyperbolic events reoccurred, which could be associated with two small, closely spaced cavities. In this case, they coincide with the estimated position of the main trace of the San José vein (Figure 2); thus, they could be more confidently associated with old surface mine workings. Because the mineralizations are lenticular and anastomosed, the first detected cavity could also be

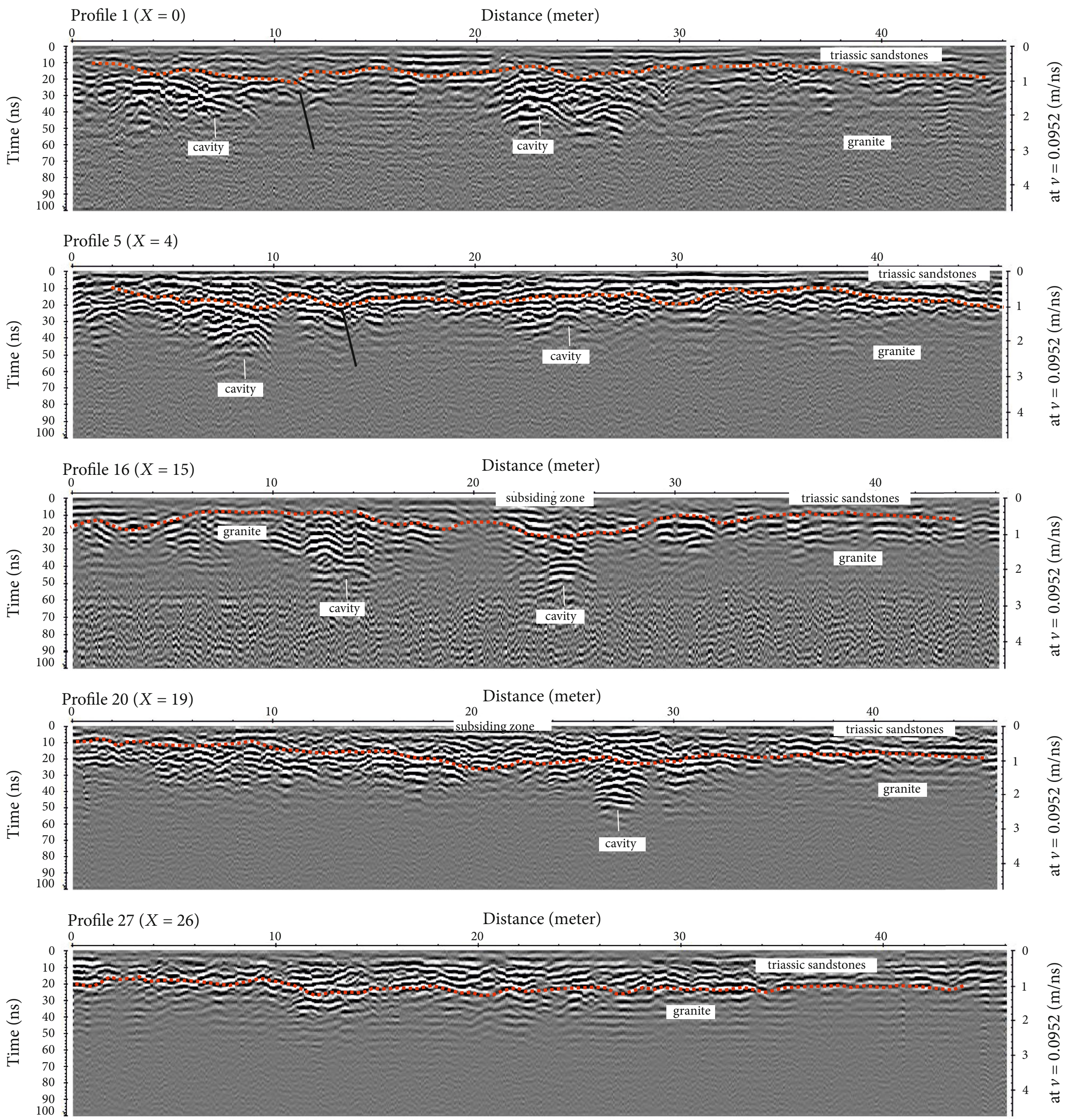

Figure 4: Radargrams in the studied sector. Explanation in the text.

associated with old mine workings. These two structures may also be in profiles 5 and 16 of Figure 4. In the latter profile, the vertical of the central cavity and a very shallow area show curved and overlapping layer morphologies, which may be associated with subsidence phenomena of approximately 0.5 m in the vertical. Recent clay sediments may fill these cavities.

In addition, Figure 4 shows profiles 1 and 5 with isolated hyperbolas and discontinuous levels, which could be associated with highly localized, small fractures. These structures may be commonly associated with these mineralizations.

The first cavity was not detected in profile 20 (Figure 4), thus suggesting that the possible excavation was not wide. Conversely, the cavity associated with the main vein was detected between 26 and 28 m from the origin and at similar depths to those discussed above. Between 20 and 28 m from the origin, morphologies of superficial layers consistent with the filling of small subsidence of approximately 0.5 m in the vertical were also detected in this cavity.

Finally, various cavities located in the previous profiles are not detected in profile 27 (Figure 4). Therefore, the extent of the vein excavations did not reach the position of this profile.

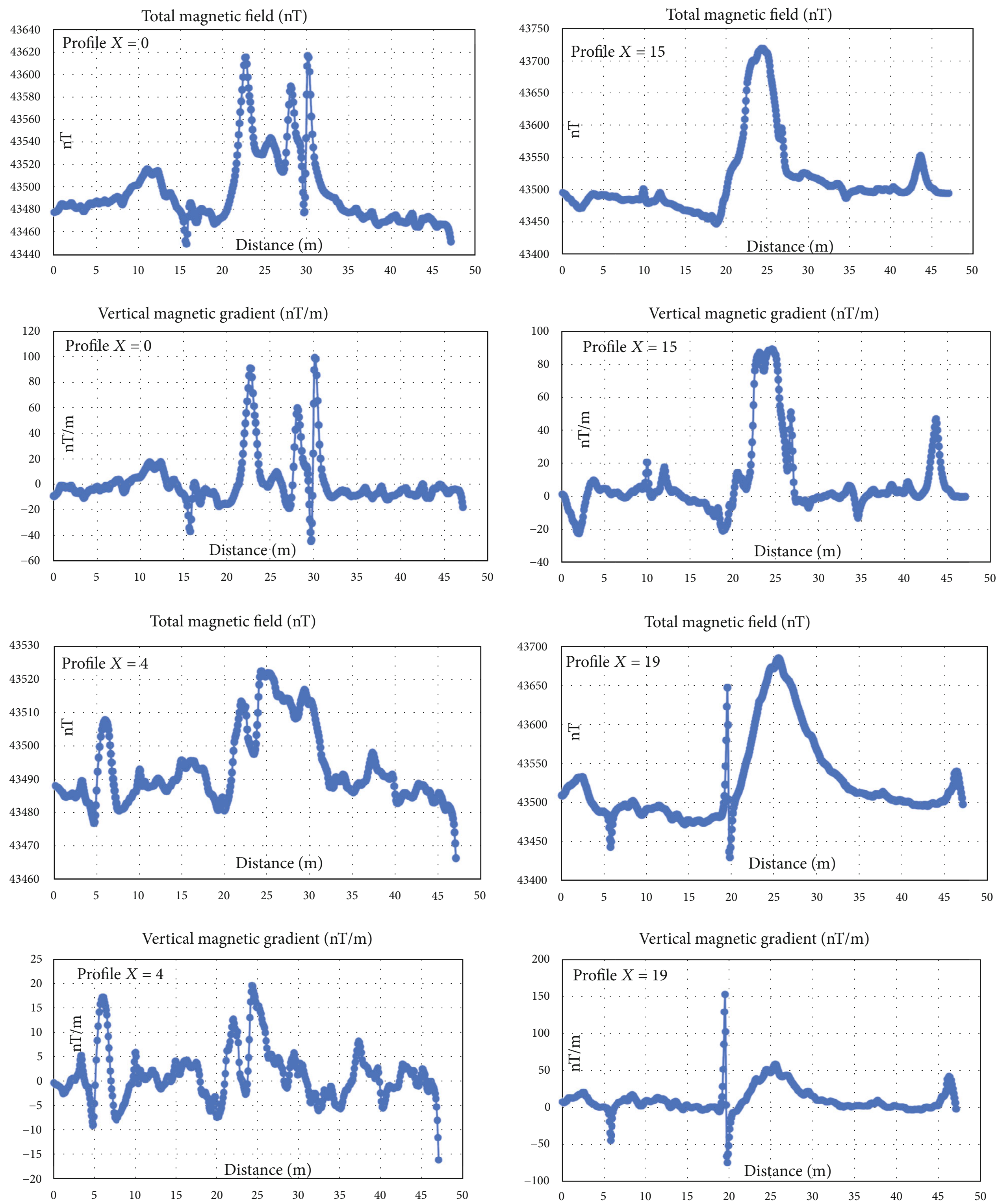

FIGURE 5: Total magnetic field profiles and vertical magnetic gradient for four profiles, which coincide with the radargrams of Figure 4 ($X = 0$, $X = 4$, $X = 15$, and $X = 19$).

5.2. Magnetic Data. Figure 5 shows four profiles in the Y-direction, whose positions match the positions in the radargrams discussed above ($X = 0$, $X = 4$, $X = 15$, and $X = 19$). The total magnetic field (expressed in nT) and the magnetic gradient (expressed in nT/m) are represented in each profile.

In all total magnetic field profiles, a maximum zone was detected between 20 and 30 m from the origin, coinciding with the trace of the vein. The value of the magnetic anomaly approximately ranged from 20 nT at $X = 4$ to 200 nT at $X = 15$ and $X = 19$ (Figure 5). Although the vein has been

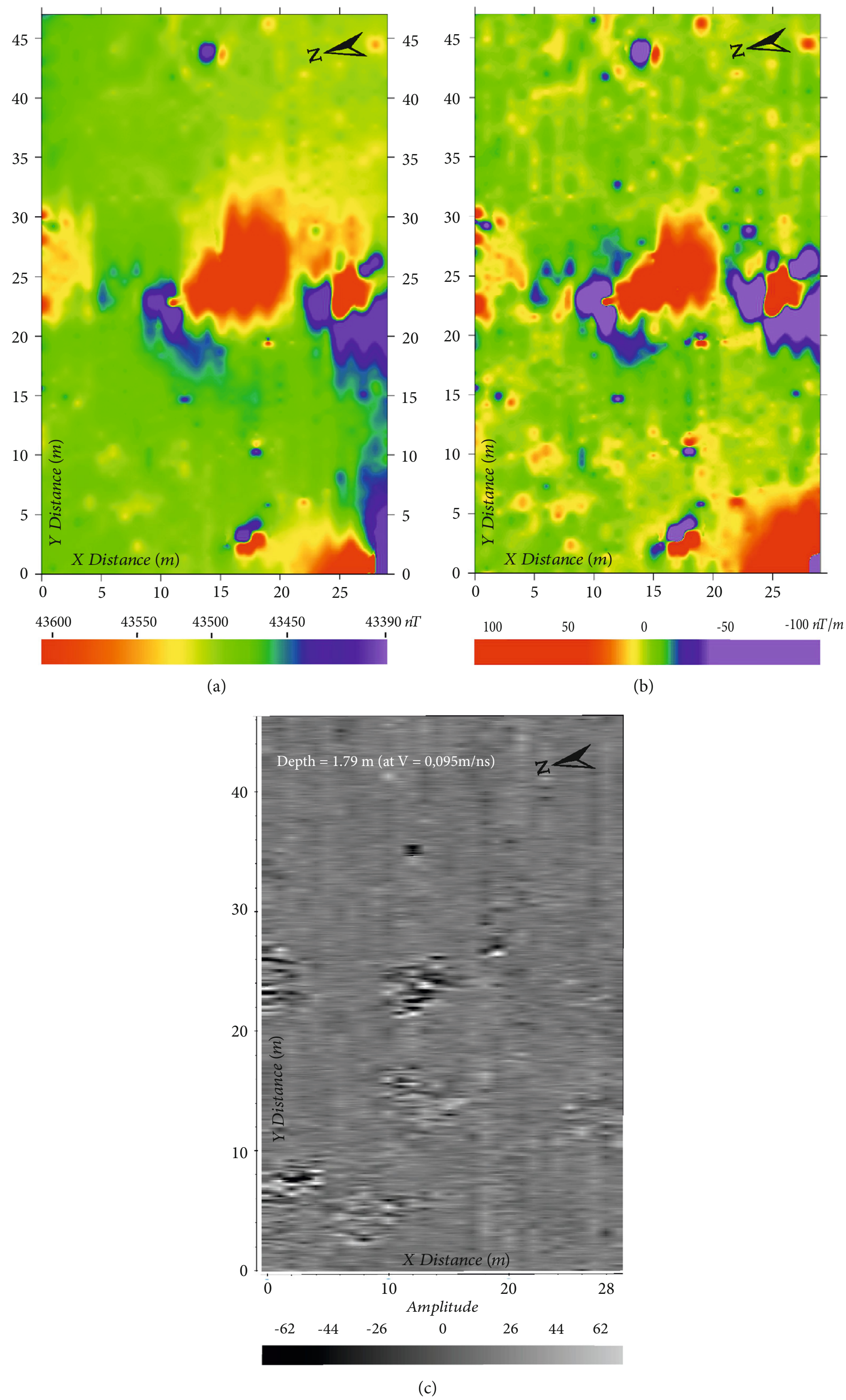

Figure 6: Plan representation of the total magnetic field (a), the vertical magnetic gradient (b), and the GPR time slice (at 37.64 ns) (c).

extensively exploited, these anomalies are associated with metal oxides and sulphides in the small remaining veins.

The cavity detected by GPR between 6 and 8 m from the origin of profile $X = 0$ was not detected in the total magnetic field profiles. A correlation with a maximum of approximately 20 nT was only possible in profile $X = 4$. This lack of correlation between the magnetic and GPR data on this point may be explained by the absence of mineralizations associated with this cavity. Conversely, in profiles $X = 15$ and $X = 19$, increases of up to 50 nT were detected between 40 and 46 m from the origin. These increases were not correlated with anomalies in GPR profiles.

When comparing total magnetic field profiles with vertical magnetic gradient profiles, no substantial differences were identified (Figure 5). The shapes of the curves were very similar, but the magnitude of the anomalies varied. In this sense, the value was usually lower when measured by the gradiometer. This difference is highlighted, for example, in profile $X = 19$, where the latter value does not exceed 50 nT/m.

The presence of remnants of unexploited mineral veins on the surface or oxide precipitates on the walls of the cavities may explain these gradient anomalies.

The total magnetic field, the vertical gradient, and the GPR time slice have been mapped in plan view for the entire grid (Figures 6(a)–6(c), respectively). The magnetic field does not show continuous anomalies associated with the trace of the vein. However, the anomalies that align along this trace enable us to detect its trajectory. This alignment could be explained by the lenticular and discontinuous mineralizations and by their exploitation processes, which removed a large part of the deposit. The position of these magnetic anomalies is confirmed in the GPR slice (Figure 6(c)) except for the right side, which is not detected in the GPR slice. This anomaly ($X = 25/Y = 22$) and the upper central anomaly ($X = 15/Y = 44$) are not detected in the GPR slice and could be related to unexploited mineralization. Furthermore, the orientation of the small dipoles is not changed.

Both surface maps show isolated anomalies in the lower area: ($X = 16/Y = 2$) and ($X = 25/Y = 1$); the anomaly in the lower right margin stands out. All the anomalies correspond to distortions due to the presence of furnace slag remnants on the surface. Their remobilisation explains the observed changes in the direction of the small magnetic dipoles, as highlighted by the gradient data shown in Figure 6(b). These anomalies are not detected in the GPR slice (Figure 6(c)) because they are not related to the cavities.

Finally, GPR slice analysis (Figure 6(c)) revealed the presence of cavities at positions $X = 4/Y = 7$, $X = 8/Y = 5$, and $X = 3/Y = 15$, which are not related to major magnetic anomalies (only very weak anomalies are detected using the gradient technique). These weak magnetic anomalies indicate that the gaps would be filled by air [22], with no mineralization present. It is possible that these cavities were excavated in an attempt to locate mineral veins but without success.

6. Conclusions

Surface cavities derived from old mining activities pose subsidence risks. Among the geophysical techniques, ground-penetrating radar and magnetometry can provide useful information about the subsurface in these regions for locating possible cavities.

Broadly, these cavities are irregular, small, and partly filled with gangue and overlying shaly material carried by water. Because of the strong dielectric contrast between the rock (granite) materials and the air of loose material filling the cavity (lutites and stones), GPR is a good method for detecting these cavities. Although the morphology cannot be described accurately, the depth of the top of the cavity, and sometimes its walls, can be assessed in GPR profiles.

Total magnetic field analysis enables us to locate a strong positive anomaly associated with the trace of the vein. Also, gradient analysis enables us to detect a strong magnetic contrast in surface areas of the trace of the vein. This anomaly is related to the presence of metallic oxides and sulphides (lead, copper, iron, zinc, barium, etc.) in the remaining small deposits or the presence of anthropogenic metallic elements that may have been buried, or even to iron oxides, that line the walls of the galleries because of precipitation associated with water percolation.

Applying these two (GPR and magnetic) techniques in the Linares mining district (Southeast Spain) confirmed that they can be used to locate old mines and identify unknown cavities. Three possibilities have been described: Firstly, cavities detected by strong dielectric contrasts correlate with strong magnetic anomalies. It would be cavities with traces of oxides. Secondly, holes are also detected due to their strong dielectric contrasts, but which are related to very weak magnetic anomalies. In this second case, they are cavities filled with air. Finally, there are sectors in which no hole has been detected by GPR, but there are strong magnetic anomalies. This response is associated either with the presence of unexploited mineralizations or with superficial smelting slag (observed in the outcrop).

Data Availability

The data that support the findings of this study are available from the corresponding author upon reasonable request.

Conflicts of Interest

The authors have not declared any conflict of interest.

Authors' Contributions

JR conceived the initial ideas of the study. RM, BM, and JR participated in the field survey. RM and BM processed and analyzed the data. RM, BM, and JR contributed to the data interpretation. RM and JR contributed to the preparation of the manuscript. All authors read and approved the final manuscript.

Acknowledgments

This study was financed by the FEDER Andalucía R+D+i Project (reference 1380520), the Ministry of Science and Innovation (Ministerio de Ciencia e Innovación—MCIN)

Project (reference PID2021-123506OB-I00), and the University of Jaén's own funds. Open Access funding is enabled and organized by CRUE-CBUA Gold.

References

[1] J. E. Azcárate, *Mapa geológico y memoria explicativa de la hoja 905 (Linares), escala 1:50.000*, Instituto Geológico y Minero de España, 1977.

[2] F. J. Larrea, M. Carracedo, L. Ortega Cuesta, and J. I. Gil Ibarguchi, "El Plutón de Linares (Jaén): cartografía, petrología y geoquímica," *Cuaderno Laboratorio Xeolóxico de Laxe Coruña*, vol. 19, pp. 335–346, 1994.

[3] M. C. Hidalgo, J. Rey, and J. Cruz San Julián, "Caracterización físico-química de los recursos hídricos de la comarca de Linares (Jaén)," in *IV Simposio del Agua de Andalucía*, pp. 89–98, Instituto Geológico y Minero de España, 1996.

[4] M. C. Hidalgo, J. Benavente, and J. Rey, "First results on the presence of metallic contaminants in waters after the abandonment of a sulphide mining district (Linares, Spain)," in *Mine, Water & Environment for the 21st Century (International Mine Water Association)*, Sevilla, 199913-17 de Septiembre de 1999.

[5] J. Cardenal, S. García-López, J. Delgado, M. C. Hidalgo, C. Marín, and J. Benavente, "Cuantificación de huecos mineros mediante técnicas de análisis de imagen. Aplicación al distrito de Linares (Jaén)," in *Patrimonio geológico y minero en el marco del Desarrollo Sostenible. Colección Temas Geológico-Mineros, vol. 31*, I. Rábano, Ed., pp. 149–158, Instituto Geológico y Minero de España, Madrid, 2000.

[6] C. Marín, J. Benavente, and J. C. Rubio, "Estimación del volumen de huecos en el batolito de Linares (Jaén)," *Geogaceta*, vol. 30, pp. 79–81, 2001.

[7] F. J. Martínez-Moreno, J. Galindo-Zaldívar, A. Pedrera et al., "Integrated geophysical methods for studying the karst system of Gruta de las Maravillas (Aracena, Southwest Spain)," *Journal of Applied Geophysics*, vol. 107, pp. 149–162, 2014.

[8] O. Pueyo-Anchuela, A. Pocoví, and A. M. Casas-Sainz, "Characterization of karst hazards from the perspective of the doline triangle using GPR—examples from central Ebro basin (Spain)," *Engineering Geology*, vol. 108, no. 3-4, pp. 225–236, 2009.

[9] F. Gutiérrez-Guzmán, *Las minas de Linares*, Apuntes históricos. Ed. Colegio Oficial de Ingenieros Técnicos de Minas de Linares, 1999.

[10] J. E. Azcárate and A. Argüelles, "Evolución Tectónica y estructuras filonianas en el distrito minero de Linares," *Congreso Hispano-Luso-Americano de Geología Económica*, vol. 4, pp. 17–32, 1971.

[11] J. Lillo, *Geology and geochemistry of Linares-La Carolina Pb-ore field (southeastern border of the Hesperian Massif), [Ph.D. thesis]*, Univ. Leeds, 1992.

[12] E. Auken, F. Jørgensen, and K. I. Sørensen, "Large-scale TEM investigation for groundwater," *Exploration Geophysics*, vol. 34, no. 3, pp. 188–194, 2003.

[13] J. L. Davis and A. P. Annan, "Ground-penetrating radar for high-resolution mapping of soil and rock stratigraphy," *Geophysical Prospecting*, vol. 37, no. 5, pp. 531–551, 1989.

[14] W. M. Telford, L. P. Geldart, and R. E. Sheriff, *Applied Geophysics*, Cambridge University Press, 2012.

[15] J. M. Reynolds, *An Introduction to Applied and Environmental Geophysics*, John Wiley and Sons Ltd., UK, 2011.

[16] A. P. Annan, "Ground Penetrating Radar: Principles, Procedures & Applications," *Sensors & Software*, vol. 278, 2003.

[17] A. Neal, "Ground-penetrating radar and its use in sedimentology: principles, problems and progress," *Earth-Science Reviews*, vol. 66, no. 3-4, pp. 261–330, 2004.

[18] O. Pueyo-Anchuela, P. Diarte-Blasco, C. García-Benito, A. M. Casas-Sainz, and J. A. Pocoví, "Geophysical and archaeological characterization of a modest Roman villa: methodological considerations about progressive feedback analyses in sites with low geophysical contrast," *Archaeological Prospection*, vol. 23, no. 2, pp. 105–123, 2016.

[19] E. Cardarelli, C. Marrone, and L. Orlando, "Evaluation of tunnel stability using integrated geophysical methods," *Journal of Applied Geophysics*, vol. 52, no. 2-3, pp. 93–102, 2002.

[20] J. L. Porsani, G. Jangelme, and R. Kipnis, "GPR survey at Lapa do Santo archaeological site, Lagoa Santa karstic region, Minas Gerais state, Brazil," *Journal of Archaeological Science*, vol. 37, no. 6, pp. 1141–1148, 2010.

[21] M. O. Ebraheem and H. A. Ibrahim, "Detection of karst features using ground-penetrating radar: a case study from the western limestone plateau, Assiut, Egypt," *Environmental Earth Sciences*, vol. 78, no. 18, p. 563, 2019.

[22] T. Mochales, E. L. Pueyo, A. M. Casas, and M. A. Soriano, "Magnetic prospection as an efficient tool for doline detection. A case study in the central Ebro basin (northern Spain)," *Geological Society of London*, vol. 279, pp. 73–84, 2017.

[23] I. Vadillo, J. Benavente, C. Neukum et al., "Surface geophysics and borehole inspection as an aid to characterizing karst voids and vadose ventilation patterns (Nerja research site, S. Spain)," *Journal of Applied Geophysics*, vol. 82, pp. 153–162, 2012.

[24] R. Blakely, *Potencial Theory in Gravity and Magnetic Applications*, Cambridge University Press, 2009.

[25] M. N. Nabighian, V. J. S. Grauch, R. O. Hansen et al., "The historical development of the magnetic method inexploration," *Geophysics*, vol. 70, pp. 33ND–61ND, 2005.

[26] M. Abedi, D. Fournier, S. Devriese, and D. W. Oldenburg, "Integrated inversion of airborne geophysics over a structural geological unit: a case study for delineation of a porphyry copper zone in Iran," *Journal of Applied Geophysics*, vol. 152, pp. 188–202, 2018.

[27] L. M. Alva-Valdivia, P. Guerrero-Díaz, J. Urrutia-Fucugauchia, A. Agarwal, and C. I. Caballero-Miranda, "Review of magmatic iron-ore mineralization in central-western Mexico: rock-magnetism and magnetic anomaly modelling of Las Truchas, case study," *Journal of South American Earth Sciences*, vol. 97, article 102409, 2020.

[28] M. Fries, M. Machado Zago, and F. Garcia da Silva, "A geophysical study contributing to analysis and characterization of a localized copper occurrence," *Journal of Applied Geophysics*, vol. 179, article 104129, 2020.

[29] M. M. Gobashy, A. Eldougdoug, M. Abdelazeem, and A. Abdelhalim, "Future development of gold mineralization utilizing integrated geology and aeromagnetic techniques: a case study in the Barramiya Mining District, Central Eastern Desert of Egypt," *Natural Resources Research*, vol. 30, pp. 2007–2028, 2021.

[30] A. Eldougdoug, M. Abdelazeem, M. Gobashy et al., "Exploring gold mineralization in altered ultramafic rocks in south Abu

Marawat, Eastern Desert, Egypt," *Scientific Reports*, vol. 13, no. 1, p. 7293, 2023.

[31] I. Murín, M. Neumann, C. Brady, J. Bátora, M. Čapo, and D. Drozda, "Application of magnetometry, georadar (GPR) and geoelectrical methods in archaeo-geophysical investigation of a Napoleonic battlefield with fortification at Pressburg (Bratislava, Slovakia)," *Journal of Applied Geophysics*, vol. 196, 2022.

[32] P. A. Peña, J. I. Manteca, P. Martínez-Pagán, and T. Teixidó, "Magnetic gradient map of the mine tailings in Portman Bay (Murcia, Spain) and its contribution to the understanding of the bay infilling process," *Journal of Applied Geophysics*, vol. 95, pp. 115–120, 2013.

[33] M. Abdelazeem and M. M. Gobashy, "A solution to unexploded ordnance detection problem from its magnetic anomaly using Kaczmarz regularization," *Interpretation*, vol. 4, no. 3, pp. SH61–SH69, 2016.

[34] K. J. Sandmeier, *REFLEXW version 7.0, program for the processing of seismic, acoustic or electromagnetic reflection, refraction and transmission data*, Software manual, Karlsruhre, Germany, 2012.